Highlights

Investigation of the Effects of Digital-to-Analog Converters on OFDM-based Modulations with Gaussian Signal Distribution

Zsolt Kollár

- Effects of DACs on multicarrier signals
- Derivation of optimal clipping ratio for uniform quantizers
- Comparison of uniform, exponential, and Lloyd–Max quantization

Investigation of the Effects of Digital-to-Analog Converters on OFDM-based Modulations with Gaussian Signal Distribution

Zsolt Kollár

Department of Artificial Intelligence and Systems Engineering, Faculty of Electrical Engineering and Informatics, Budapest University of Technology and Economics, Műegyetem rkp. 3., H-1111 Budapest, Hungary

ARTICLE INFO

Keywords:
DAC
Quantization
SDQR
OFDM
Multicarrier

ABSTRACT

This paper investigates the impact of Digital-to-Analog Converters (DACs) on the generation of multicarrier signals, with a focus on Orthogonal Frequency Division Multiplexing (OFDM). A mathematical framework is developed to model DAC behavior in this context, and its performance is analytically evaluated. First, a closed-form expression is derived for the optimal clipping threshold under uniform quantization, expressed as a function of DAC bit resolution. Then, an improved optimization strategy is introduced for allocating non-uniform quantization levels to maximize the Signal-to-Distortion and Quantization Ratio (SDQR) at the DAC output. An upper bound on SDQR is further established using the Lloyd–Max quantization method. The influence of these quantization schemes on overall system performance—including bit error rate and spectral characteristics—is also assessed. The results apply to multicarrier systems with Gaussian-distributed signals and can be extended to related communication and signal-processing scenarios.

1. Introduction

Complex-valued multisine signals play a pivotal role in the implementation of modern multicarrier modulation schemes, most notably in Orthogonal Frequency Division Multiplexing (OFDM) systems [1]. These signals are fundamental to a broad class of communication technologies that fall under the umbrella of OFDM-based systems, such as Filter Bank MultiCarrier (FBMC) [2], Generalized Frequency Division Multiplexing (GFDM) [3], and the more recently introduced Orthogonal Time Frequency Space (OTFS) modulation techniques [4]. In these systems, both the real and imaginary components of the complex baseband signal can be interpreted as independent multicarrier signals, each comprising numerous subcarriers modulated in parallel across the frequency spectrum.

The discrete-time domain representation of these multicarrier signals can be generated efficiently through the use of the Inverse Fast Fourier Transform (IFFT), which synthesizes the time-domain waveform from its frequency-domain subcarrier components. Conversely, signal analysis and demodulation at the receiver side are typically performed using the Fast Fourier Transform (FFT), which enables the extraction of individual subcarriers and facilitates signal processing tasks such as channel equalization and symbol detection.

Different OFDM variants often incorporate additional filtering stages or transformation techniques to address specific performance requirements or limitations. For example, FBMC utilizes filter banks to enhance spectral localization and minimize intercarrier interference, whereas GFDM introduces flexibility in time-frequency resource allocation. OTFS, on the other hand, aims to provide robustness in highly dispersive wireless channels by modulating information in the delay-Doppler domain.

One inherent property of multicarrier signals is that they are composed of a large number of sinusoidal components, whose amplitudes and phases vary independently. Due to the central limit theorem [5], the resulting composite time-domain signal tends to exhibit a Gaussian-like amplitude distribution. This statistical characteristic implies that, with high probability, occasional large signal peaks may appear—significantly exceeding the average signal power. Such peaks give rise to a high Peak-to-Average Power Ratio (PAPR), which presents a major challenge in practical transmitter implementations. High PAPR forces power amplifiers to operate with a large back-off from their saturation point to maintain linearity, leading to substantial reductions in power efficiency. Alternatively, operating the amplifier near or in the nonlinear region introduces signal distortions and unwanted spectral regrowth, resulting in Out-Of-Band (OOB) emissions that can interfere with adjacent channels.

To mitigate the negative effects of high PAPR, various signal processing techniques have been proposed, including clipping, tone reservation, selective mapping, and active constellation extension, among others. These methods aim to reduce the dynamic range of the signal while minimizing the degradation in Bit Error Rate (BER) and spectral efficiency.

An additional and equally critical step in the transmitter chain of a multicarrier system is the conversion of the digitally generated time-domain samples into an analog waveform suitable for radio-frequency transmission. This task is performed by the Digital-to-Analog Converter (DAC), whose performance significantly influences the quality and fidelity of the transmitted signal. However, DACs are inherently constrained by factors such as limited input range (due to voltage swing restrictions) and finite resolution (determined by the number of quantization bits). When high PAPR signals are fed into such DACs, clipping and quantization

*Corresponding author
kollarzs@mit.bme.hu (Z. Kollár)
https://www.mit.bme.hu/en/staff/kollarzs (Z. Kollár)
ORCID(s): 0000-0001-6384-265X (Z. Kollár)

effects can introduce distortion and noise, which degrade system performance.

The impact of Digital-to-Analog Converters (DACs) with uniform quantization on multicarrier signals has been previously discussed in the literature [1]. A non-uniform quantization scheme for DACs applied to multisine signals was introduced in [6], with simulation results demonstrating that the Signal-to-Distortion-Quality-Ratio (SDQR) can be significantly enhanced by employing such DACs. In [7], a low-bit resolution DAC with non-uniform quantization levels was utilized, leveraging the statistical distribution of the multisine signal to improve the SDQR. Further, [8] presents both analytical and simulation results examining the influence of DACs on the performance of complex multisines, along with a novel technique for mitigating the impact of the DAC on the SDQR. Additionally, optimization strategies for Analog-to-Digital Converters (ADCs) in the context of Gaussian input signals were explored in [9], where bit resolution and clipping levels were optimized using numerical methods. This paper extends these investigations by focusing on optimizing both the clipping level and quantization levels to maximize the SDQR at the DAC output, utilizing a combination of analytical methods and simulations.

This paper investigates how the limitations of Digital-to-Analog Converters (DACs) affect the quality of multicarrier waveforms, focusing on the combined impact of finite amplitude range and quantization resolution on the time-domain Signal-to-Distortion and Quantization Ratio (SDQR). Because OFDM-based signals exhibit a near-Gaussian amplitude distribution, their high-PAPR nature makes them especially sensitive to clipping and quantization effects. Using a two-stage DAC model -—comprising amplitude clipping followed by uniform quantization -— an analytical expression is derived for the attenuation factor, clipping noise, and quantization error, enabling a closed-form characterization of SDQR as a function of the clipping ratio and bit-resolution. This framework reveals an inherent trade-off between clipping distortion and quantization noise, from which an optimal clipping ratio is obtained for any given number of bits. The analysis is further extended to non-uniform quantization. An upper performance bound is established via Lloyd–Max optimization, and a practical exponential quantizer is evaluated as a hardware-feasible alternative. Both approaches outperform uniform quantization by allocating finer resolution to the statistically dense central region of the Gaussian signal. Overall, the results demonstrate that DAC performance in multicarrier systems can be significantly enhanced by tailoring clipping thresholds and quantization levels to the signal's amplitude distribution, thereby reducing distortion and improving signal integrity in practical OFDM and related waveforms.

The generation of digital baseband multicarrier signals is detailed in Section 2. Section 3 provides an overview of the Digital-to-Analog Converter (DAC) model, addressing constraints related to the limited input range and resolution. In addition, an optimal selection of parameters for uniform quantization is derived. The potential application of non-uniform quantization is explored in Section 4. The effects of the discussed quantizers on the overall system performance are investigated in Section 5. Finally, Section 6 synthesizes the findings and presents the conclusions.

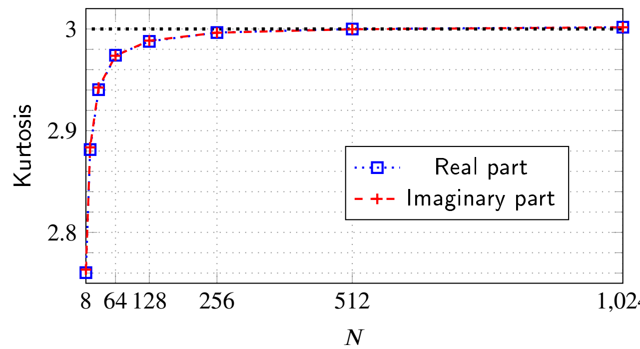

Figure 1: The value of the kurtosis for the real and imaginary parts ($x_{\Re}[n]$ and $x_{\Im}[n]$) of the OFDM signal as a function of N, $N_c = N/2$.

2. OFDM-based signals

The complex baseband time-domain samples – with normalized sampling time – of a periodic complex multicarrier signal with a period of N samples is defined as

$$s[n] = s_{\Re}[n] + s_{\Im}[n] = \sum_{k=1}^{N_c} C_k e^{j2\pi f_k n}, \quad (1)$$
$$0 \le n \le N-1, N_c \le N,$$

where N_c is the number of modulated frequencies and Quadrature Amplitude Modulation (QAM) value $C_k = |C_k|e^{j\varphi_k}$ where $\varphi_k = \angle C_k$ is the phase of the k^{th} tone. With the choice of $f_k = k/N$, the frequencies are spaced equidistantly, and the generation of the signal can be performed via IFFT.

As the OFDM signal is a multicarrier waveform, the central limit theorem implies that the amplitude distribution of its real and imaginary components can be approximated as Gaussian. To verify this assumption, the kurtosis of the real and imaginary parts of the OFDM signal was analyzed. Kurtosis indicates the shape of a signal distribution; for a normal distribution, the kurtosis equals 3. Figure 1 shows the kurtosis of the real and imaginary parts of the OFDM signal as a function of N, where $N_c = N/2$ denotes the number of used subcarriers. It can be observed that the kurtosis values approach 3 for both components [10]. Hence, when using more than 128 subcarriers, the real and imaginary parts of the OFDM signal can be regarded as Gaussian. This fact will be crucial in modeling the DAC for OFDM signals.

A real-valued multicarrier signal is a special case of (1) when the following holds:

$$C_k = C^*_{N-k}, \quad (2)$$

Table 1
Simulation parameters for OFDM signal.

Parameter	Value
Modulation type	64-QAM
Number of carriers (N)	512
Number of subcarriers (N_c)	256
Number of symbols	10000

where C^* denotes the complex conjugate of C. The resulting real-valued multicarrier signal with period N can be expressed as

$$s[n] = \sum_{k=1}^{N_c} A_k \cos(2\pi f_k n + \varphi_k), \quad 0 \le n \le N-1, N_c \le N/2, \tag{3}$$

where $A_k = 2|C_k|$, f_k and φ_k are the amplitude, frequency and initial phase of the k^{th} frequency.

Other OFDM-based modulations such as FBMC, OTFS, and GFDM, use preprocessing or transformations on the modulation symbols C_k or further filtering on the time domain signal, but this still leads to a Gaussian distribution of the time domain signal.

In all simulation experiments discussed in this paper, the parameters listed in Table 1 were applied. For the Monte-Carlo simulations, the OFDM signal was generated as follows: 10,000 OFDM symbols were produced, with 128 out of 256 subcarriers in each symbol modulated using 64-QAM (6 bits per symbol). This corresponds to a total binary data length of $6 \times 128 \times 10{,}000 = 7{,}680{,}000$ bits.

3. Modeling the DAC

In this section, the model of the DAC is presented using clipping and quantization steps. Considering the input signal $s[n]$, the SDQR is given at the output. The investigated multicarrier signal generation is depicted in Fig. 2 with the multicarrier modulation and the DACs. The model of the DAC can also be observed: the limited input range can be considered as clipping, and the finite bit resolution is modeled as quantization. In case of complex multicarrier signals, the real and imaginary parts are treated separately, thus using 2 DACs.

3.1. Clipping

The clipped signal for the real component of the complex baseband signal can be expressed based on the clipping level $A_{\max}$ of the DAC as

$$s^c_{\Re}[n] = \begin{cases} +A_{\max}, & \text{if } s_{\Re}[n] \ge +A_{\max}, \\ s_{\Re}[n], & \text{if } -A_{\max} < s_{\Re}[n] < +A_{\max}, \\ -A_{\max}, & \text{if } s_{\Re}[n] \le -A_{\max}. \end{cases} \tag{4}$$

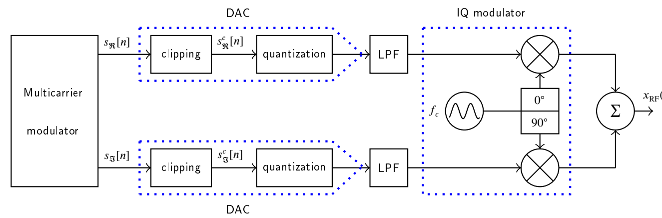

Figure 2: Block diagram of a multicarrier transmitter.

The clipping ratio is defined as

$$\gamma = \frac{A_{\max}}{\sigma_{s_{\Re}}}, \tag{5}$$

where $\sigma_{s_{\Re}}$ is the square root of the average power $P_{s_{\Re}}$ of the input signal prior to clipping. According to the Bussgang theorem, as long as the input signal is considered Gaussian distributed, the clipped signal can be given as [11]

$$s^c_{\Re}[n] = \alpha s_{\Re}[n] + d[n], \tag{6}$$

where the attenuation factor α can be expressed with the error function as

$$\alpha = \operatorname{erf}\left(\frac{\gamma}{\sqrt{2}}\right), \tag{7}$$

and $d[n]$ is the clipping noise uncorrelated with the input signal. According to [11], the power of the clipped signal can be calculated with the aid of the complementary error function as

$$P_{s^c_{\Re}} = \left(1 - \sqrt{\frac{2}{\pi}}\gamma e^{-\frac{\gamma^2}{2}} - (1-\gamma^2)\operatorname{erfc}\left(\frac{\gamma}{\sqrt{2}}\right)\right) P_{s_{\Re}}. \tag{8}$$

Furthermore, the power of the clipping noise using (6) and (8) can be expressed as

$$\begin{aligned} P_d &= P_{s^c_{\Re}} - \alpha^2 P_{s_{\Re}} = \\ &= \left(1 - \sqrt{\frac{2}{\pi}}\gamma e^{-\frac{\gamma^2}{2}} - (1-\gamma^2)\operatorname{erfc}\left(\frac{\gamma}{\sqrt{2}}\right) \right. \\ &\left. \quad -\operatorname{erf}^2\left(\frac{\gamma}{\sqrt{2}}\right)\right) P_{s_{\Re}}. \end{aligned} \tag{9}$$

The value of α and P_d as a function of the CR are shown in Fig. 3. It can be seen that above 12 dB, the value of α approaches 1, and P_d approaches zero; thus, no clipping occurs from the signal.

Finally, the Signal-to-Distortion Ratio (SDR) after amplitude limitation can be expressed using (6) and (9) as

$$\begin{aligned} \mathrm{SDR} &= \frac{\alpha^2 P_{s_{\Re}}}{P_d} \\ &= \frac{\operatorname{erf}^2\left(\frac{\gamma}{\sqrt{2}}\right)}{1-\sqrt{\frac{2}{\pi}}\gamma e^{-\frac{\gamma^2}{2}}-(1-\gamma^2)\operatorname{erfc}\left(\frac{\gamma}{\sqrt{2}}\right)-\operatorname{erf}^2\left(\frac{\gamma}{\sqrt{2}}\right)}. \end{aligned} \tag{10}$$

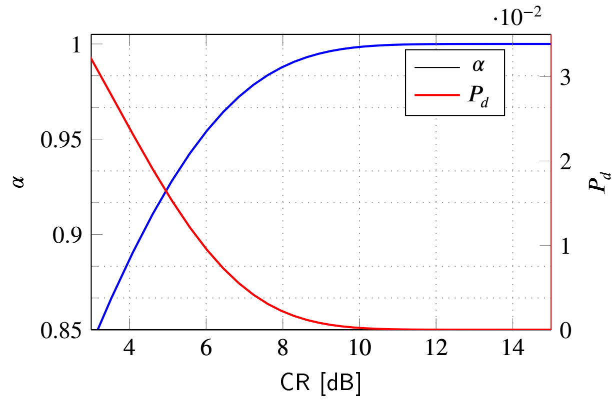

Figure 3: The value of α and P_d as function of CR.

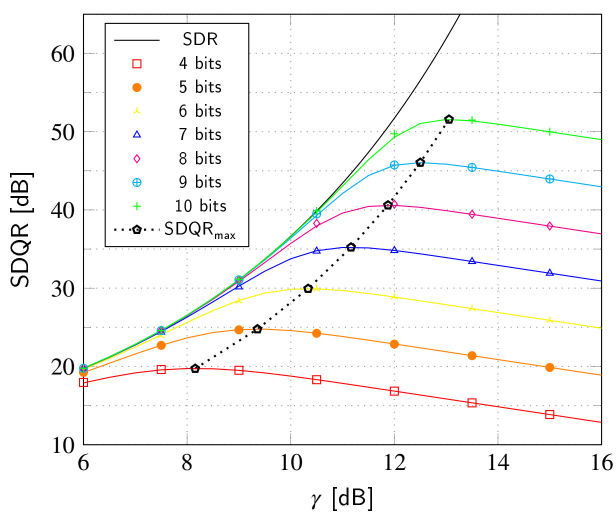

Figure 4: Theoretical SDQR (solid lines) and simulated SDQR (markers) as a function of γ for different number of quantization bits.

3.2. Uniform quantization

The clipped signal is quantized in the second step of modeling the DAC. The resolution of the quantizer determines the dynamic range and the transition levels. The output voltage can be expressed based on the digital code D and the Full Scale Range (FSR) of the DAC output:

$$A_{\text{out}} = \text{sign}(D)\frac{A_{\text{FSR}}}{2D_{\max}}D, \tag{11}$$

where $D = -D_{\max}, \dots, D_{\max} - 1$, with $D \in \mathbb{Z}$, $D_{\max} = 2^{f_b - 1}$ where f_b being the number of bits used in the quantization and $A_{\text{FSR}} = 2A_{\max}$. The quantization noise power assuming uniform quantization is given by [12]

$$P_{\text{Q}} = \frac{q^2}{12}, \tag{12}$$

where

$$q = \frac{A_{\text{FSR}}}{2^{f_b}} \tag{13}$$

is the ideal quantization step. The quantization noise power can be determined as a function of the power of the input signal $P_{s_{\mathfrak{R}}}$ using γ and (12) as

$$P_{\text{Q}} = \frac{\frac{4A_{\max}^2}{2^{2f_b}}}{12} = \frac{\gamma^2 P_{s_{\mathfrak{R}}}}{3 \cdot 2^{2f_b}}. \tag{14}$$

The resulting SDQR based on (9) and (14) is given by

$$\text{SDQR}(\gamma, f_b) = \frac{\alpha^2 P_{s_{\mathfrak{R}}}}{P_d + P_Q}$$

$$= \frac{\text{erf}^2\left(\frac{\gamma}{\sqrt{2}}\right)}{1-\sqrt{\frac{2}{\pi}}\gamma e^{-\frac{\gamma^2}{2}}-(1-\gamma^2)\text{erfc}\left(\frac{\gamma}{\sqrt{2}}\right)-\text{erf}^2\left(\frac{\gamma}{\sqrt{2}}\right)+\frac{\gamma^2}{3\cdot 2^{2f_b}}}. \tag{15}$$

The simulated and theoretical SDQR as a function of γ for different bit resolutions f_b are presented in Fig. 4. It is observed that at lower values of γ, clipping noise dominates the system's behavior. However, beyond a certain optimal γ, quantization error becomes the predominant factor. Additionally, the data indicate that there exists an optimal γ value for each bit resolution, where the SDQR reaches its maximum. As the number of bits increases, this optimal γ value shifts toward higher clipping ratios, suggesting a relationship between bit resolution and the optimal balance between clipping noise and quantization error.

As the statistical characteristics of the signals $s_{\mathfrak{I}}$ and $s_{\mathfrak{R}}$ are similar, the same calculations presented through equations (4)-(15) apply for $s_{\mathfrak{I}}$ as well.

3.3. Optimal γ for uniform quantization

Observing Fig. 4, it can be stated that for a given bit-resolution, an optimal clipping γ_{opt} can be determined for which the output SDQR can be maximized. To find the optimal value of γ which maximizes the SDQR for a given bit resolution f_b:

$$\gamma_{\text{opt}} = f\left(f_b\right), \tag{16}$$

the SDQR must be differentiated with respect to γ and solved for the value 0:

$$\frac{\partial \text{SDQR}(\gamma, f_b)}{\partial \gamma} = 0. \tag{17}$$

The analytical derivative is expressed in (18). A graphical visualization of the formula is given in Fig. 5. As can be seen, the zero crossing of the function shifts towards higher γ with enlarged f_b. Although the function seems to be smooth, it exhibits extremely large values with higher f_b values. Furthermore, as the expression is not directly solvable for γ, a different approach is suggested: the equation is rearranged, and instead of γ, it is solved for 2^{2f_b}. Thus, the inverse function $f_b = f^{-1}(\gamma_{\text{opt}})$ is expressed as shown in (19). This function is depicted in Fig 6. Numerical analysis revealed that the relationship between γ_{opt} and f_b is approximately a

$$\frac{2^{2f_b}3\mathrm{erf}\left(\frac{\gamma}{\sqrt{2}}\right)\left(-2\pi e^{\gamma^2}\gamma\mathrm{erf}\left(\frac{\gamma}{\sqrt{2}}\right)\left(2^{2f_b}3\mathrm{erfc}\left(\frac{\gamma}{\sqrt{2}}\right)+1\right)+2\sqrt{2\pi}e^{\frac{\gamma^2}{2}}\left(\gamma^2+2^{2f_b}3\left(\left(\gamma^2-1\right)\mathrm{erfc}\left(\frac{\gamma}{\sqrt{2}}\right)+1\right)\right)-12\gamma 2^{2f_b}\right)}{\left(\sqrt{\pi}e^{\frac{\gamma^2}{2}}\left(\gamma^2+2^{2f_b}3\left(\gamma^2+\mathrm{erf}\left(\frac{\gamma}{\sqrt{2}}\right)\right)\mathrm{erfc}\left(\frac{\gamma}{\sqrt{2}}\right)\right)-2^{2f_b}3\sqrt{2}\gamma\right)^2}=0 \tag{18}$$

$$2^{2f_b}=\frac{\sqrt{2\pi}e^{\frac{\gamma^2}{2}}\gamma^2-\pi e^{\gamma^2}\gamma\mathrm{erf}\left(\frac{\gamma}{\sqrt{2}}\right)}{3\left(-\sqrt{2\pi}e^{\frac{\gamma^2}{2}}+2\gamma+\pi e^{\gamma^2}\gamma\mathrm{erf}\left(\frac{\gamma}{\sqrt{2}}\right)\mathrm{erfc}\left(\frac{\gamma}{\sqrt{2}}\right)+\sqrt{2\pi}\left(-e^{\frac{\gamma^2}{2}}\right)\gamma^2\mathrm{erfc}\left(\frac{\gamma}{\sqrt{2}}\right)+\sqrt{2\pi}e^{\frac{\gamma^2}{2}}\mathrm{erfc}\left(\frac{\gamma}{\sqrt{2}}\right)\right)}. \tag{19}$$

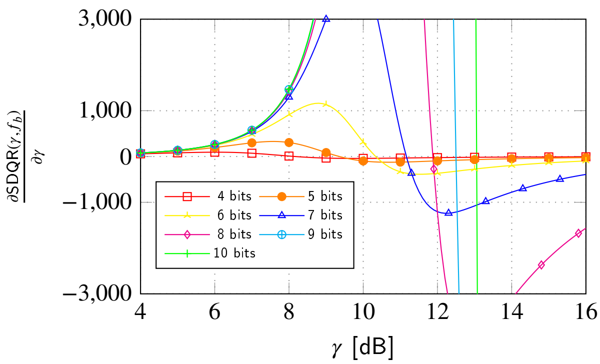

Figure 5: The value of Equation (18) in function of γ and f_b.

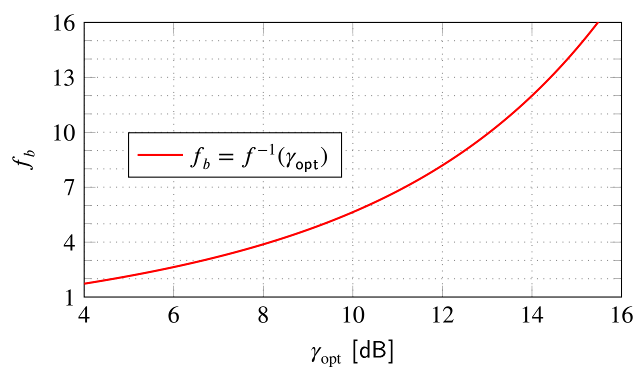

Figure 6: The value of $f_b = f^{-1}(\gamma_{\mathrm{opt}})$ expressed by Equation (19).

power function – with logarithmic scaling, the map of the relation is very close to a straight line – thus, the searched expression can be given as

$$\log_{10}\gamma_{\mathrm{opt}} \approx \log_{10}a + c\log_{10}f_b, \tag{20}$$

that is, between $\log_{10}\gamma_{\mathrm{opt}}$ and $\log_{10}f_b$ there is approximately a linear relation. The task is to express the constants a and c. For this, $\log_{10}f_b$ is expressed as a function of $\log_{10}\gamma_{\mathrm{opt}}$, then $\log_{10}\gamma_{\mathrm{opt}}$ is linearized by Taylor-series expansion, and finally, this linear relation is inverted to express $\log_{10}\gamma_{\mathrm{opt}}$ as a function of $\log_{10}f_b$. To perform this, the logarithm of both sides of (19) needs to be taken twice (in this way, on the left-hand side, $\log_{10}f_b$ appears). Then, the series expansion of

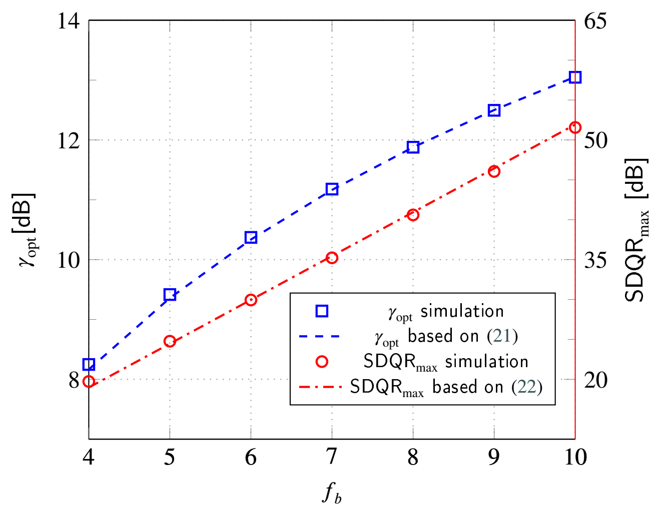

Figure 7: The value of the optimal clipping ratio (left axis) and the corresponding maximum SDQR (right axis) as a function of f_b for uniform quantizers.

the right side with respect to $\log_{10}\gamma$ is differentiated around a suitable value of γ in the investigated range. After linearizing (taking the first two terms in the series expansion of) the right-hand side of the equation around the value of $\gamma = 4.5 =$ 13dB . Finally the expression for γ_{opt} is obtained as follows

$$20\log_{10}\gamma_{\mathrm{opt}} \approx 0.979 + 12.074\log_{10}f_b. \tag{21}$$

Furthermore, the theoretically achievable maximum SDQR for a given bit resolution at γ_{opt} can be calculated by evaluating (15) using (21). After linearization, the maximum SDQR in the function of f_b can be expressed:

$$\mathrm{SDQR}_{\mathrm{max}}[\mathrm{dB}] = 10\log_{10}\mathrm{SDQR}_{\mathrm{max}} \approx 5.45f_b - 3.008. \tag{22}$$

It can be observed in Fig. 7 that the derived theoretical curves closely approximate the results obtained by numerical simulations. Furthermore, due to the Gaussian nature of the input signal and clipping effects, a gain of approximately 5.5 dB/bit can be achieved compared to DACs, where a 6 dB/bit increase in signal-to-quantization noise can be expected.

4. Applying non-uniform quantization

The possible application of non-uniform quantization to improve the SDQR is investigated in this section. The objective is to minimize the following expression with $p(x)$ being the Probability Density Function (PDF) [13]:

$$\min_{x_q} \sum_{q=1}^{2^{f_b}} \int_{t_{q-1}}^{t_q} (x - x_q)^2 p(x)\mathrm{d}x, \text{ s.t. } x_{q+1} > x_q. \quad (23)$$

Thus, the optimal placement of the quantized values x_q must be found within the decision interval $[t_{q-1}, t_q)$.

The Lloyd-Max algorithm is an iterative procedure for minimizing the SDQR of a signal with a given PDF and a specified number of decision intervals and levels. Such an optimal quantizer is referred to as a Lloyd-Max quantizer [13]. Although the Max–Lloyd algorithm provides the theoretically optimal non-uniform quantizer for a given source probability distribution, its direct implementation as a non-uniform analog DAC is not practical. The resulting design would require custom, irregular threshold networks and precisely spaced, non-uniform output levels, which are highly sensitive to process variations and temperature fluctuations. Consequently, contemporary systems implement Max–Lloyd quantization entirely in the digital domain, using look-up tables or arithmetic mappings, and rely on a conventional uniform DAC for the analog reconstruction.

An exponential quantizer is a non-uniform scalar quantizer whose decision thresholds and output levels grow exponentially with the index. It is a simpler, closed-form alternative to Max–Lloyd quantizers when the source statistics are strongly peaked near zero and have long tails (e.g., Gaussian-like, Laplacian, or exponential distributions). Thus, a suboptimal solution uses an exponential quantizer, for which values near zero are quantized with finer resolution than values near the FSR. Such quantizers are often used in acoustic-, bio-, radio frequency- signal-processing [13, 14, 15]. For the evaluation, – in contrast to the uniform quantizer given in (11) –, the following transfer function was selected for the DAC output:

$$A_{\mathrm{out}} = \mathrm{sign}(D)\frac{A_{\mathrm{FSR}}}{2e^{0.5(D_{\max}-1)}}e^{0.5(D-1)}. \quad (24)$$

The transfer function of the Lloyd-Max and the exponential DAC is depicted in Fig. 8 for $f_b = 7$ bits. It can be observed that both quantizers have a high resolution for low values and a larger resolution for higher values. The resulting SDQR in the function of γ with different bit resolutions can be seen in Fig. 9, and it can be observed that both non-uniform quantizers outperform the uniform one, the gap between them becomes more dominant with larger f_b.

In Fig. 11, the SDQR gain using non-uniform quantizers over the uniform one in the function of f_b is visualized, where the superiority of the Lloyd-Max quantizer becomes even more dominant. In case of higher bit resolutions further optimization of the exponential quantizer is required to better approximate the results of the Lloyd-Max quantizer.

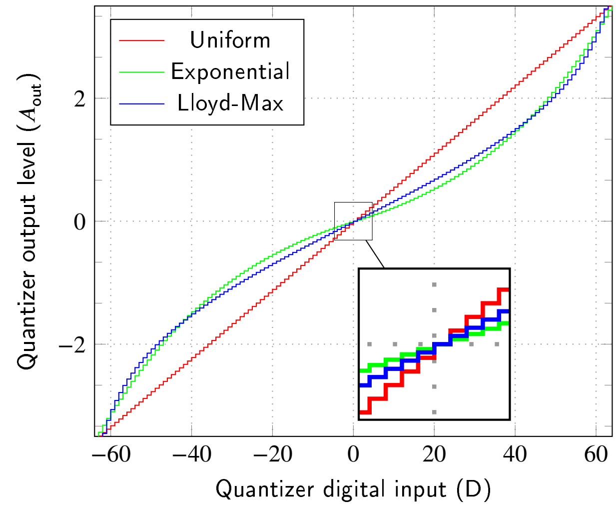

Figure 8: Transfer function for uniform and non-uniform quantizers with $f_b = 7$ bits and $\gamma = \gamma_{\mathrm{opt}}$.

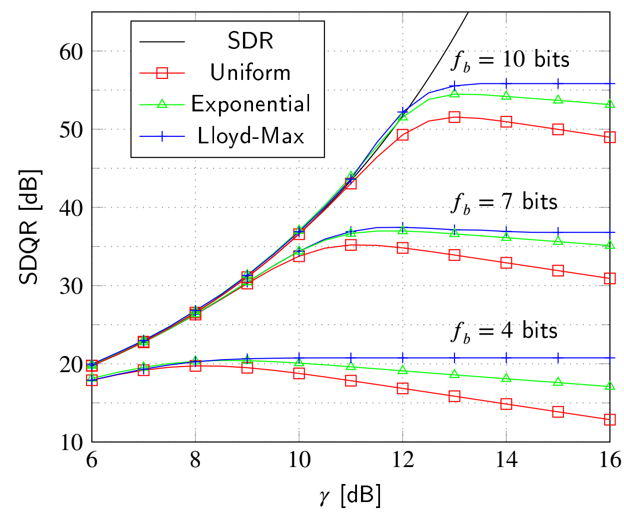

Figure 9: Simulated SDQR as a function of γ for different numbers of quantization bits and different types of quantizers.

5. System performance

In this section, the impact of the previously discussed quantization effects on the overall system performance, specifically in terms of BER and Power Spectrum Density (PSD), is evaluated. In addition to the simulation parameters listed in Table 1, the following settings are applied: for OFDM, a cyclic prefix (N_{CP}) of 32 samples is used; for FBMC, the Phydyas prototype filter [16] with an overlapping factor of 4 is employed. All other system components, including the receiver and demodulation algorithms, are assumed to be ideal.

The theoretical BER [17] in function of the system parameters for M-QAM modified with the SDQR model is

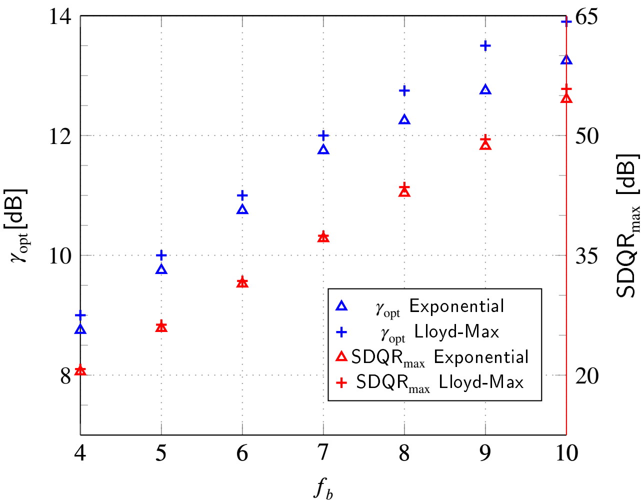

Figure 10: The value of the optimal clipping ratio (left axis) and the corresponding maximum SDQR (right axis) as a function of f_b for nonuniform quantizers.

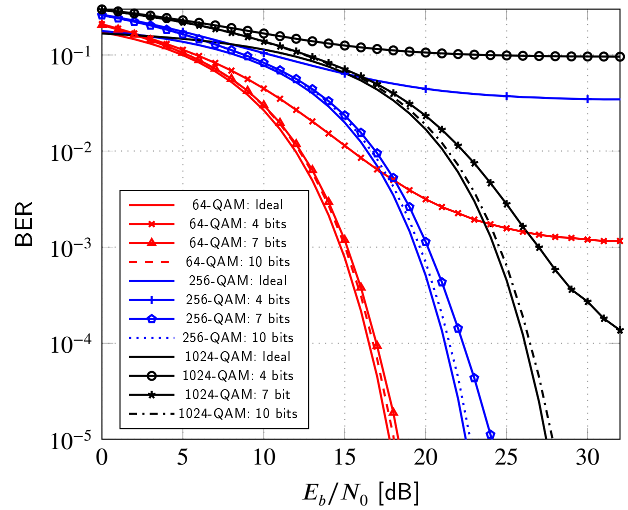

Figure 12: Bit-error rate curves with different quantization bits for uniformly quantized OFDM signal over AWGN channel in function of E_b/N_0. for 64-, 256- and 1024-QAM.

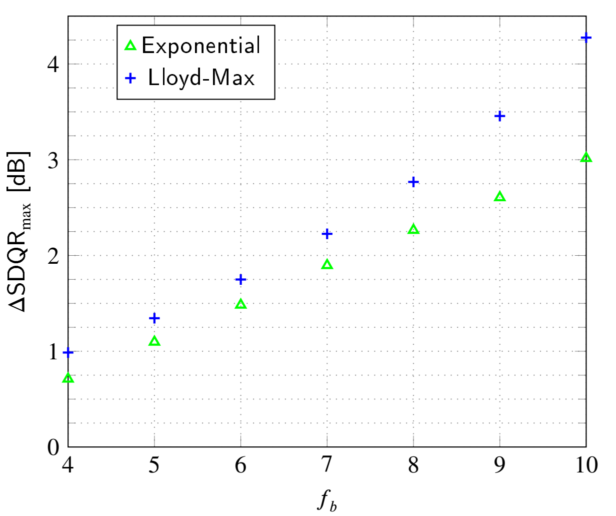

Figure 11: The gain in SDQR for the exponential and Lloyd-Max quantizer compared to the uniform quantizer as a function of f_b.

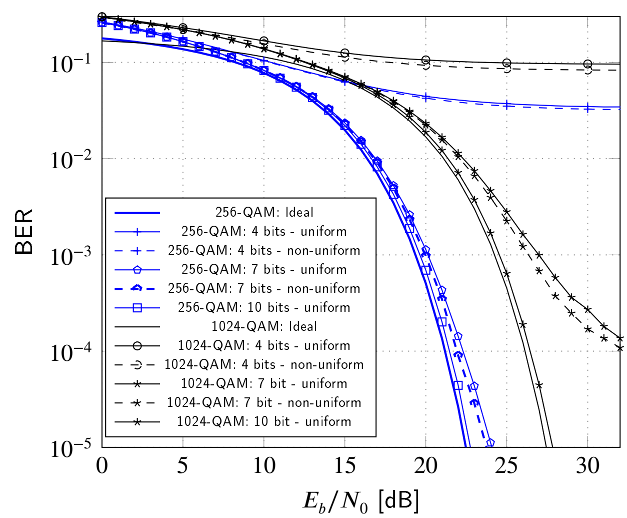

Figure 13: Bit-error rate curves with different quantization bits using uniform and non-uniform (Lloyd-Max) quantizer for OFDM signal over AWGN channel in function of E_b/N_0 for 256- and 1024-QAM.

expressed as

$$\mathrm{BER} = \frac{2}{\log_2 M}\left(1-\frac{1}{\sqrt{M}}\right)\cdot \mathrm{erfc}\left(\sqrt{\frac{3\log_2 M}{2(M-1)}\frac{N_c}{N+N_{\mathrm{CP}}}\frac{\alpha E_s}{N_0+P_d+P_Q}}\right), \tag{25}$$

where M is the QAM order and N_0 denotes the noise power.

Fig. 12 shows the BER performance over an Additive White Gaussian Noise (AWGN) channel for 64-, 256-, and 1024-QAM using uniform quantizer. As expected, the impact of quantization error is relatively small for low-order constellations, whereas for high-order QAM the quantization noise becomes dominant, leading to error floors.

To evaluate the benefits of non-uniform quantizers, the BER performance of 256- and 1024-QAM over an AWGN channel is compared with that of uniform quantizers in Fig. 13. The results indicate that the BER improvement is minimal at low resolutions, becomes slightly more noticeable at 7 bits, and for 10 bits, the BER achieved with non-uniform quantizers matches the ideal performance curve.

Fig. 14 shows the PSD of the OFDM and FBMC signals under different quantization bit resolutions. The distortions introduced by quantization increase the OOB emissions. For OFDM, 7 bit quantization is sufficient to reach the OOB

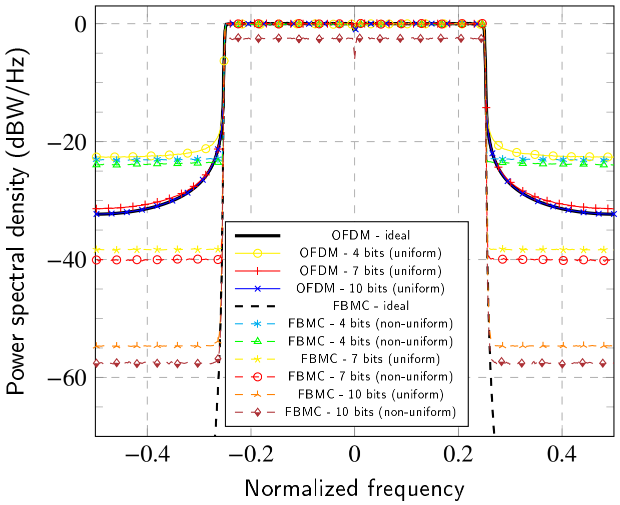

Figure 14: Power spectrum density function of the FBMC/OFDM signal with different quantization bits and optimal clipping ratio in case of uniform and non-uniform (Lloyd-Max) quantizers.

level of the ideal, unquantized OFDM signal; using 10 bits provides no additional benefit, since the OOB emissions are limited by the OFDM sidelobes caused by the rectangular pulse shaping. In contrast, the FBMC signal exhibits inherently lower OOB emissions, so applying 7 bit or 10 bit quantization still results in improved OOB performance compared to OFDM. Furthermore, using a non-uniform quantizer for FBMC can reduce the OOB emissions even more compared to the uniform quantization case.

6. Conclusion

This paper investigates how DAC parameters influence OFDM-based signals that exhibit a Gaussian distribution. It explores the trade-off between clipping distortion and quantization noise, from which an optimal uniform quantization strategy that maximizes the SDQR is derived. Further improvements to the SDQR are demonstrated through the use of non-uniform quantization. An upper bound is determined using the Lloyd–Max quantizer, and a practical suboptimal approach is introduced via an exponential quantizer.

The impact of these quantizers on overall system performance is evaluated through simulation. The results show that low-resolution quantizers can lead to BER saturation and substantially degrade the PSD, thereby increasing OOB emissions. For smaller QAM constellations, quantization effects are less severe on the BER performance; moreover, for OFDM, the spectral shape can be largely preserved even with 7-bit quantizers. However, in advanced communication systems employing high-order QAM and requiring low OOB emissions, higher-resolution DACs become necessary. The analytical expressions developed in this work provide a basis for defining system requirements and offer valuable guidance for DAC design in multicarrier systems, including OFDM, FBMC, GFDM, and OTFS.

Acknowledgment

The research presented in this paper is partially funded by the National Research, Development, and Innovation Office (NKFIH) through the OTKA Grant (K 142845), and by the János Bolyai Research Grant (BO/00042/23/6) of the Hungarian Academy of Sciences. The author would like to thank also Monther Alrwashdeh and Prof. József Bíró for their helpful comments.

Declaration of generative AI and AI-assisted technologies in the writing process

During the preparation of this work, the authors used Grammarly and OpenAI-ChatGPT to improve readability and language. After using these tools, the authors reviewed and edited the content as necessary, taking full responsibility for the publication's content.

References

[1] C. R. Berger, Y. Benlachtar, R. I. Killey, Optimum Clipping for Optical OFDM with Limited Resolution DAC/ADC, in: Advanced Photonics, Optica Publishing Group, 2011, p. SPMB5. doi:10.1364/SPPCOM.2011.SPMB5.

[2] Z. Kollár, M. Alrwashdeh, L. Leitold, Performance analysis of FBMC signals in the presence of DACs with limited range and resolution, in: 34th International Conference Radioelektronika (RADIOELEKTRONIKA), 2024, pp. 1–5. doi:10.1109/RADIOELEKTRONIKA61599.2024.10524059.

[3] G. Fettweis, M. Krondorf, S. Bittner, GFDM - generalized frequency division multiplexing, in: VTC Spring 2009 - IEEE 69th Vehicular Technology Conference, 2009, pp. 1–4. doi:10.1109/VETECS.2009.5073571.

[4] M. Aldababsa, S. Özyurt, G. K. Kurt, O. Kucur, A survey on orthogonal time frequency space modulation, IEEE Open Journal of the Communications Society 5 (2024) 4483–4518.

[5] H. Yoo, F. Guilloud, R. Pyndiah, Amplitude PDF analysis of OFDM signal using probabilistic papr reduction method, EURASIP Journal on Wireless Communications and Networking 2011 (2011).

[6] T. Huang, M. Bi, G. Yang, L. Liu, X. Miao, H. He, S. Xiao, W. Hu, Nonuniform quantification DAC for improving the performance of IMDD-based FBMC system, in: 16th International Conference on Optical Communications and Networks (ICOCN), 2017, pp. 1–3. doi:10.1109/ICOCN.2017.8121561.

[7] J. Peng, L. Han, Q. Zhu, C. Qiu, Y. Zhang, C. Tremblay, Y. Su, SQNR Improvement Enabled by Nonuniform DAC Output Levels for IM-DD OFDM Systems, IEEE Photonics Journal 9 (2017) 1–11.

[8] M. Bernhard, D. Rörich, T. Handte, J. Speidel, Analytical and numerical studies of quantization effects in coherent optical OFDM transmission with 100 Gbit/s and beyond, in: 13th ITG Symposium on Photonic Networks, 2012.

[9] Y. Hou, G. Liu, Q. Wang, W. Xiang, Performance optimization of digital spectrum analyzer with gaussian input signal, IEEE Signal Processing Letters 20 (2013) 31–34.

[10] W. Qiu, W. J. Murphy, A. Suter, Kurtosis: a new tool for noise analysis, Acoust Today 16 (2020) 39–47.

[11] A. Frömming, L. Häring, A. Czylwik, Spectral properties of clipping noise, Mathematics 9 (2021).

[12] B. Widrow, I. Kollár, Quantization Noise: Roundoff Error in Digital Computation, Signal Processing, Control, and Communications, Cambridge University Press, Cambridge, UK, 2008.

[13] Y. You, Audio Coding: Theory and Applications, Springer Science and Business Media LLC, 2010. doi:10.1007/978-1-4419-1754-6.

[14] L. Danial, K. Sharma, S. Dwivedi, S. Kvatinsky, Logarithmic neural network data converters using memristors for biomedical applications, in: 2019 IEEE Biomedical Circuits and Systems Conference (BioCAS), 2019, pp. 1–4. doi:10.1109/BIOCAS.2019.8919068.

[15] A. Esmailiyan, E. Ghaderi, I. Ghotbi, O. Shoaei, A CMOS pseudo-exponential current-output DAC with code-dependent body-biasing, Analog Integr. Circuits Signal Process. 88 (2016) 127–136.

[16] S. K. Shaikhah, S. Mustafa, A robust filter bank multicarrier system as a candidate for 5G, Physical Communication 43 (2020) 101228.

[17] H. Bouhadda, H. Shaiek, D. Roviras, R. Zayani, Y. Medjahdi, R. Bouallegue, Theoretical analysis of BER performance of non-linearly amplified FBMC/OQAM and OFDM signals, EURASIP Journal on Advances in Signal Processing 2014 (2014) 60.